Chinese Chemical Letters 36 (2025) 109641

Contents lists available at ScienceDirect

Chinese Chemical Letters

journal homepage: www.elsevier.com/locate/cclet

A cationic radical lanthanide organic tetrahedron with remarkable coordination enhanced radical stability

Zhengzhong Zhu[a,b], Shaojun Hu[a,b], Zhi Liu[a], Lipeng Zhou[a,b], Chongbin Tian[a,b,*], Qingfu Sun[a,b,*]

[a] State Key Laboratory of Structural Chemistry, Fujian Institute of Research on the Structure of Matter, Chinese Academy of Sciences, Fuzhou 350002, China
[b] University of the Chinese Academy of Sciences, Beijing 100049, China

ARTICLE INFO

Article history:
Received 15 January 2024
Revised 30 January 2024
Accepted 7 February 2024
Available online 13 February 2024

Keywords:
Supramolecular chemistry
Self–assembly
Lanthanide organic polyhedrons
Radical
Enhanced stability

ABSTRACT

Rare–earth supramolecular compounds, such as lanthanide organic polyhedrons (LOPs), are of particular interest due to their many possible applications in various fields. Here we report the first syntheses of $Ln_4(L^{\bullet+})_4$–type (Ln, lanthanides; $L^{\bullet+}$, radical ligand) radical–bridged lanthanide organic tetrahedrons by self–assembly of face–capping triphenylamine (TPA)–cored radical ligand with different lanthanide ions. Remarkable coordination enhanced radical stability has been observed, with half–life times ($t_{1/2}$) for $L_1^{\bullet+}$, $La_4(L_1^{\bullet+})_4$, $Eu_4(L_1^{\bullet+})_4$, $Gd_4(L_1^{\bullet+})_4$, $Tb_4(L_1^{\bullet+})_4$ and $Lu_4(L_1^{\bullet+})_4$ estimated to be 53 min, 482 min, 624 min, 1248 min, 822 min and 347 min, respectively. The TPA radical in $Ln_4(L_1^{\bullet+})_4$ containing paramagnetic Ln ions (Ln = Eu^{III}, Gd^{III} and Tb^{III}) is observed to be more stable than that in $Ln_4(L_1^{\bullet+})_4$ (Ln = La^{III} and Lu^{III}) constructed by diamagnetic Ln ions. This difference in radical stability is possibly due to the magnetic interactions between paramagnetic Ln^{III} ions and $L_1^{\bullet+}$ ligands, as confirmed by electron paramagnetic resonance (EPR) in $La_4(L)_4$ (L = L_1 and $L_1^{\bullet+}$) and $Tb_4(L)_4$ (L = L_1 and $L_1^{\bullet+}$), and magnetic susceptibility measurements in $Tb_4(L)_4$ (L = L_1 and $L_1^{\bullet+}$). Our study reveals the coordination of radical ligands with lanthanide ions can improve the radical stability, which is crucial for their applications.

Coordination–driven self–assembly, a fascinating synthetic strategy in supramolecular chemistry, is widely used to prepare a variety of discrete metallosupramolecular architectures, including helicates, macrocycles/wheels and cages/capsules [1–6]. So far, the majority of the coordination–supramolecular architectures are based on transition metal ions [7–22], such as Pd^{II}, Pt^{II}, Fe^{II}, Au^{I}, Ag^{I} and Zn^{II}, while architectures containing lanthanide [23–27] are less explored. This is mainly due to the difficulty in controlling the coordination number and geometry of Ln^{III} ions, which have variable and labile coordination habits. However, lanthanide supramolecular compounds have attractive optical and magnetic properties derived from the 4f electrons, which make them valuable for functional exploration. Our research group has been devoted to the synthesis and study of lanthanide organic polyhedrons (LOPs) since 2015 [24]. Along with other groups, we have successfully prepared several types of Ln_2L_3 helicates, Ln_4L_4 tetrahedrons and Ln_8L_6 cubes [23,24] with particular interests toward their luminescence, cell imaging, chirality, and catalysis [23,28–33]. However, all reported LOPs are synthesized by diamagnetic closed–shell ligands. Incorporating radical–containing ligands into the multi–component assemblies can provide a new platform to examine multiple spin–spin magnetic interactions and access novel functions that are unavailable in single radical systems [34–37]. To the best of our knowledge, no examples of such radical lanthanide polyhedrons exist.

Organic radical species are prone to disproportion or intermolecular dimerization. It had been demonstrated that covalent approach was an effectively method to improve the stability of organic radicals by using bulky substituents for steric protection or introducing conjugated groups [38,39], polar substituents [40] or heteroatoms [41] to delocalize the spin density. To prevent the dimerization, non–covalent strategy, also known as supramolecular approach, mainly relies on host–guest chemistry [42–44] and non–covalent interactions, such as hydrogen bonds [45], electrostatic interaction [46], π–π interaction [47]. Apart from these, coordination bonds were found to enhance the organic radicals' stability. For example, Wang and co–works demonstrated that metal–coordination can synergistically stabilize the radical cations of the main group elements [48]. Moreover, recent reports have also revealed that the coordination of radical ligands to transition metal ions could gener-

* Corresponding authors.
E-mail addresses: tianchongbin@fjirsm.ac.cn (C. Tian), qfsun@fjirsm.ac.cn (Q. Sun).

https://doi.org/10.1016/j.cclet.2024.109641
1001-8417/

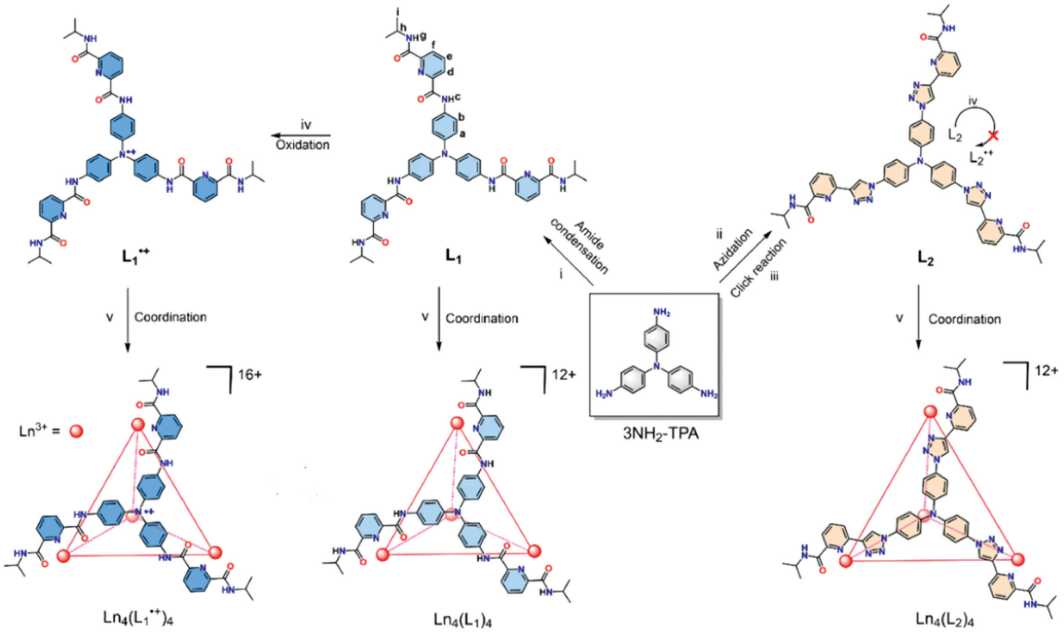

Scheme 1. Synthetic route of TPA–bridging ligands L_1, L_2, $L_1^{\bullet+}$ and self–assembly of $Ln_4(L)_4$ tetrahedral cages. (i) 6–(Isopropylcarbamoyl)picolinic acid, HATU, Et_3N, 70% yield, (ii) $NaNO_2$/HCl, NaN_3, (iii) 6–ethynyl–*N*–isopropylpicolinamide, SA, $CuSO_4{\cdot}5H_2O$, 75% yield, (iv) $NOBF_4$, 95% yield, (v) $Ln(OTf)_3$, 99% yield.

ate impressive radical stability in metallacycles [49–51]. However, combining radical ligand with metal organic polyhedrons aimed at improving the radical stability was rarely investigated [52–54], in particular by coordination with lanthanide ions.

Triphenylamine (TPA) radical cations and its derivatives, obtained by one–electron oxidation of triphenylamine, have been extensively applied in a wide range of areas, including organic and hybrid solar cells, organic redox catalysis, magnetic materials, *etc.* [54–66]. Herein, we report the first $Ln_4(L^{\bullet+})_4$–type (Ln = La^{III}, Eu^{III} and Tb^{III}) radical–bridged lanthanide organic tetrahedrons synthesized from self–assembly of face–capping TPA–cored radical ligand with Ln ions (Scheme 1). TPA–cored cationic radical ligand $L_1^{\bullet+}$ features three peripheral electron–donating pyridine diamide chelating sites at para position. For an facilitate–intuitive comparison, L_2 with a triazolyl group replacing inner amide group on L_1, and its $Ln_4(L_2)_4$ assemblies were also synthesized. However, it was observed that L_2 failed to oxidize into its radical form. All compounds have been well characterized by ^{1}H NMR, DOSY and ESI–TOF–MS. Moreover, the structure of $Eu_4(L_1)_4$, $Eu_4(L_1^{\bullet+})_4$ and $Eu_4(L_2)_4$ have been unambiguously confirmed by X–ray crystallographic analyses, wherein $Eu_4(L_1^{\bullet+})_4$ represents the first example of radical LOPs. The generation of radical cations, their stability and lanthanide–radical magnetic interaction were further studied by UV−vis−NIR, CV, EPR spectra, magnetic susceptibilities measurements, together with density functional theory (DFT) calculations. After coordination with lanthanide ions, the enhanced radical half–life time of $L_1^{\bullet+}$ in $Ln_4(L_1^{\bullet+})_4$ assemblies was observed. Remarkably, $Eu_4(L_1^{\bullet+})_4$, $Tb_4(L_1^{\bullet+})_4$, and $Tb_4(L_1^{\bullet+})_4$ exhibit much longer radical half–life time than that of $La_4(L_1^{\bullet+})_4$ and $Lu_4(L_1^{\bullet+})_4$, likely due to the magnetic interactions between paramagnetic Ln^{III} ions and $L_1^{\bullet+}$.

Ligand L_1 was readily synthesized by a one–step amide condensation reaction between 6–(isopropylcarbamoyl)picolinic acid and a C_3–symmetric tri(4–amino)triphenylamine ($3NH_2$–TPA) core. As a control, ligand L_2 was prepared by the Click reaction (Scheme 1, Scheme S1 and S2, Figs. S1–S4, S9 and S10 in Supporting information).

When ligand was treated with 1 equiv. of $Ln(OTf)_3$ in acetonitrile solution at room temperature for serval minutes, the turbid suspension of the ligand quickly turned into a clear solution, indicating the generation of new species. Taking L_1 as an example, NMR and ESI–TOF–MS spectra show the formation of a high symmetric $Eu_4(L_1)_4$ species (Fig. 1, Figs. S5 and S6 in Supporting information). Compared to free L_1, characteristic upfield shifts for $H_{c\text{-}g}$ on the chelating moieties of L_1 are clearly observed (Fig. 1b), while H_a and H_b on TPA core are shifting downfield, consistent with the coordination of chelating moieties with Eu^{III} ions. Moreover, the signal of H_i on the terminal isopropyl splits into two doublets with equal integration, implying a rigid coordination configuration. The ^{1}H diffusion–ordered NMR spectroscopy (DOSY, Fig. 1c) displays the presence of sole product with a hydrodynamic diameter of 3.2 nm. As shown in Fig. 1d, high resolution ESI–TOF–MS analyses confirm the formation of the assembly with a chemical formula of $Eu_4(L_1)_4(OTf)_{12}$. A series of prominent peaks with charging states from 3+ to 6+ derived by the successive loss of OTf^- counterions and active hydrogen on the amide of $Eu_4(L_1)_4(OTf)_{12}$ are observed. For instance, peak with $m/z = 898.8013$ corresponds to the $[Eu_4(L_1)_4(OTf)_{12}–H_4–(OTf)_9]^{5+}$ charged species (Fig. 1d, inset). After replacing Eu^{III} ion with La^{III} or Tb^{III} ions, ^{1}H NMR spectrum and/or the ESI–TOF–MS also confirmed the formation of $La_4(L_1)_4$ and $Tb_4(L_1)_4$ (Figs. S7, S14 and S17 in Supporting information). The analogous $Eu_4(L_2)_4$ complex was also synthesized in a similar way for comparison purpose (Fig. S11 in Supporting information).

Single crystals of the $Eu_4(L_1)_4$ and $Eu_4(L_2)_4$ assemblies were grown by slow vapor diffusion of diethyl ether into their acetonitrile solution, confirming their tetrahedral geometry (Figs. 1e and f), which are isomorphic to our previous reported Eu_4L_4–type tetrahedral cages [67,68]. The four metal centers on the tetrahedron display cooperative ΔΔΔΔ or ΛΛΛΛ chirality, and both enantiomers coexist in crystals (Figs. S20–S22 in Supporting information), as they all crystallize in the achiral Fm-3 space group. In the crystal structures of $Eu_4(L_1)_4$ and $Eu_4(L_2)_4$, each Eu^{III} centers are nine–coordinated and ligated by three chelating moieties from three different ligands.

To investigate the redox properties of the free ligands and their assemblies, we initially oxidized the neutral ligand with nitrosonium tetrafluoroborate ($NOBF_4$), a common one–electron oxidant. Upon addition of $NOBF_4$, the solution color of L_1 in acetonitrile

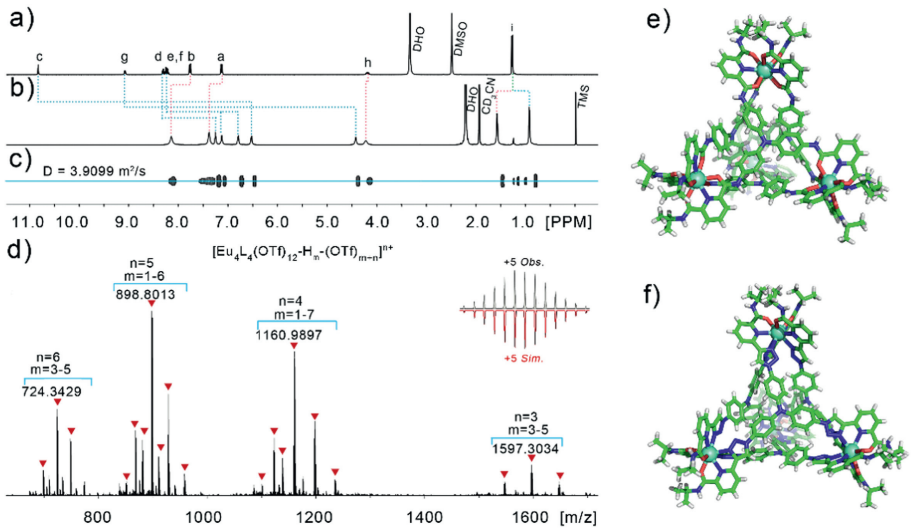

Fig. 1. ^{1}H NMR of (a) ligand L_1 in DMSO–d_6 and (b) tetrahedral cage $Eu_4(L_1)_4(OTf)_{12}$ in CD_3CN. (c) ^{1}H DOSY spectrum of $Eu_4(L_1)_4(OTf)_{12}$. (d) ESI–TOF–MS of $Eu_4(L_1)_4(OTf)_{12}$ with insets showing the observed (Obs.) and simulated (Sim.) isotopic patterns for the 5+ peaks. Single crystal X–ray structures of (e) $Eu_4(L_1)_4$ and (f) $Eu_4(L_2)_4$. Eu: Cyan, C: green, N: blue, O: red, H: white.

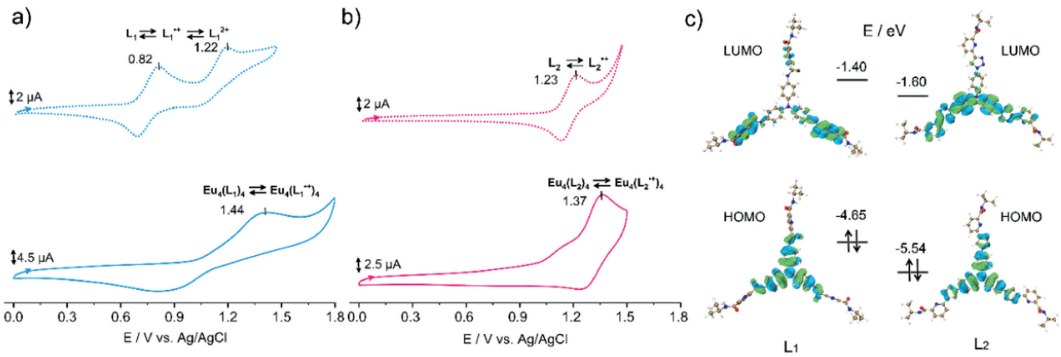

Fig. 2. (a, b) Cyclic voltammetry of ligand L_1, $Eu_4(L_1)_4$ and L_2, $Eu_4(L_2)_4$ (1 mmol/L for ligands, 0.25 mmol/L for cages, 0.1 mol/L $^nBu_4NPF_6$, scan rate 100 mV/s) at room temperature. (c) Frontier orbitals of L_1 and L_2 calculated using DFT methods (B3LYP/6–31G(d)).

rapidly changed from yellow to green, which is a characteristic color of TPA–cored radical cation, indicating the generation of $L_1^{\bullet+}$. The formation of radical cation was also unambiguously confirmed by the UV–vis and EPR spectra (*vide infra*). It should be noted that the ^{1}H NMR spectra of $L_1^{\bullet+}$ were significantly broadened, due to the paramagnetic nature of the radical species on the TPA units (Fig. S4). Unfortunately, we failed to produce the radical cation $L_2^{\bullet+}$ using several reported efficient oxidation reagents, including $NOBF_4$, $Cu(ClO_4)_2$ and $AgBF_4$, suggesting its high oxidation potential.

To elucidate the distinction between L_1 and L_2, cyclic voltammetry (CV) was measured for both ligands in DMSO containing tetrabutylammonium hexafluorophosphate ($^nBu_4NPF_6$) at a scan rate of 100 mV/s (*vs.* Ag/AgCl) under an argon atmosphere. Free ligand L_1 exhibited one reversible oxidation wave around +0.82 V and an irreversible oxidation peak around +1.22 V, corresponding to the formation of $L_1^{\bullet+}$ and L_1^{2+}, respectively (Fig. 2a). Similar CV waves were observed for $L_1^{\bullet+}$ (Fig. S48 in Supporting information), which further confirmed the assignment of the oxidation peaks and the stability of the radical cation form. However, only one reversible oxidation wave was observed around +1.23 V for ligand L_2 (Fig. 2b), which was even higher than the second oxidation potential of L_1. We also calculated the frontier orbitals of ligands L_1 and L_2 using DFT methods at the UB3LYP/6–31G(d) level of theory to explain the different behavior under electrochemical condition. Fig. 2c shows that the energy of the HOMO (HOMO = highest occupied molecular orbital) of L_2 (–5.54 eV) is lower than L_1 (–4.65 eV) by 0.89 eV [69]. This lower delocalized HOMO indicates weaker electron loss ability, which is in good agreement with the higher first reversible oxidation potential (E^{ox}) of L_2, consistent with the CV results (E^{ox} (L_1) = 0.82 V *vs.* E^{ox} (L_2) = 1.23 V). Moreover, we performed the CV experiments for $Eu_4(L_1)_4$ and $Eu_4(L_2)_4$ in acetonitrile. Compared with $L_1^{\bullet+}$, only one broadened oxidation wave was observed for the cage $Eu_4(L_1)_4$ with a positive shift of the oxidation potential around +1.44 V, likely due to the complexation with Eu^{III} and the polycationic nature (12+) of the Ln^{III}–linked cage structure [52,70]. This behavior demonstrates the considerable stability of the $Eu_4(L_1^{\bullet+})_4$ radical cage as well as the absence of disassembly during the redox process. In sharp contrast, only one irreversible oxidation wave was observed around 1.37 V in the $Eu_4(L_2)_4$ acetonitrile solution.

Next, we examined the assembly of $L_1^{\bullet+}$ with Ln ions. We obtained a clear assembly solution by mixing the radical cation $L_1^{\bullet+}$ with $Eu(OTf)_3$ in acetonitrile. The UV–vis spectrum of this solution showed three absorption peaks, two of which (under 500 nm) were similar to the absorption peaks of $Eu_4(L_1)_4$, indicating the formation of $Eu_4(L_1^{\bullet+})_4$ (Fig. S34 in Supporting information). It should be noted that a new shoulder peak at about 735 nm in $Eu_4(L_1^{\bullet+})_4$ was observed compared to $Eu_4(L_1)_4$. To verify this difference, we measured the UV–vis absorption of L_1 and $L_1^{\bullet+}$ in the same solution (Fig. 3a). Unlike L_1, a typical radical absorption peak around 784 nm was found in $L_1^{\bullet+}$, in agreement with the reported TPA

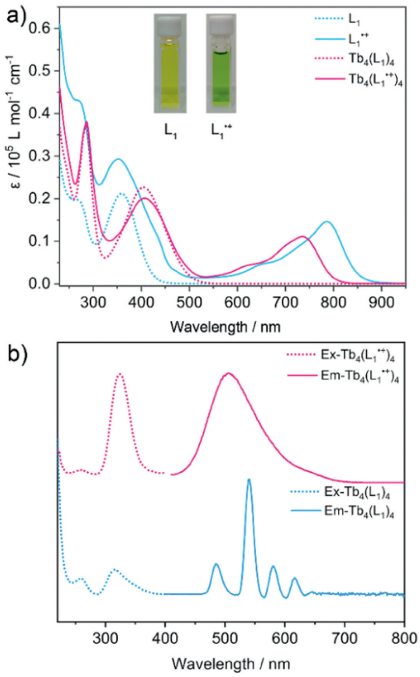

Fig. 3. (a) Absorption spectra of L_1 (0.1 mmol/L, blue dot line), $L_1^{\bullet+}$ (0.1 mmol/L, blue line), $Tb_4(L_1)_4$ (0.025 mmol/L, pink dot line), $Tb_4(L_1^{\bullet+})_4$ (0.025 mmol/L, pink line) in CH_3CN, Inset: the color view of L_1 and $L_1^{\bullet+}$. (b) Excitation and emission spectra of $Tb_4(L_1)_4$ (blue line) and $Tb_4(L_1^{\bullet+})_4$ (pink line) in CH_3CN.

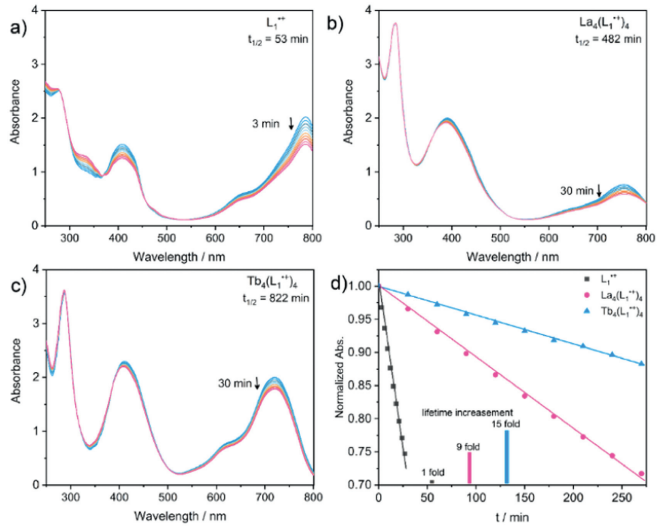

Fig. 4. Time–dependent UV–vis absorption spectra of (a) $L_1^{\bullet+}$, (b) $La_4(L_1^{\bullet+})_4$ and (c) $Tb_4(L_1^{\bullet+})_4$ in CH_3CN recorded at ambient air and light conditions. (d) Plot of the absorbance at 784 nm ($L_1^{\bullet+}$), 760 nm ($La_4(L_1^{\bullet+})_4$), 740 nm ($Tb_4(L_1^{\bullet+})_4$) with time, showing the half–life times were increased by 9–fold and 15–fold for $La_4(L_1^{\bullet+})_4$, $Tb_4(L_1^{\bullet+})_4$, respectively.

radical cation [71]. Therefore, the new peak observed in $Eu_4(L_1^{\bullet+})_4$ could be attributed to the absorption band of the radical ligands $L_1^{\bullet+}$ (Fig. S34), and its slight blue shift in $Eu_4(L_1^{\bullet+})_4$ may be caused by the coordination with Eu^{III} ions. Similarly, the successful preparation of $La_4(L_1^{\bullet+})_4$ and $Tb_4(L_1^{\bullet+})_4$ was also confirmed by the UV–vis spectra (Fig. 3a and Fig. S34). We failed to obtain ESI–TOF–MS data for the radical assemblies $Ln_4(L_1^{\bullet+})_4$ (Ln = La, Eu and Tb), which may be due to their easy reduction under the ionization conditions.

Interestingly, the greenish cubic single crystals (Fig. S21) of the radical assembly were grown overnight by the same vapor diffusion method as for the $Eu_4(L_1)_4$ crystal growth process. Like $Eu_4(L_1)_4$, this radical cage also crystalizes in the cubic space group F_m-3. The main difference lies in their C–N bond length on the TPA panels. This bond length in the radical cage (1.404 Å, Fig. S28 in Supporting information) is shorter by about 0.015 Å than that in cage $Eu_4(L_1)_4$ (1.419 Å), similar to the trends observed in the mono–radical cation of thiophene–bridged bis(TPA) [72], indicative of the radical feature of TPA panels in radical cage. The single crystal structure provides reliable evidence for the existence of radical centers in a tetrahedral cage. However, the crystal structure cannot confirm that each tetrahedral cage contains four radicals, due to the easy recovery feature of TPA-type radical during the crystal growth process. According to the calculated half–life time from UV–vis tracking experiment (*vide infra*) coupled with the crystal growth time, we speculate that about 2 radicals may be remained in a cage after the crystallization process.

The spin density distribution of $L_1^{\bullet+}$ was estimated by DFT calculations at the UB3LYP/6–31G(d) level of theory. Spin density of $L_1^{\bullet+}$ was found to be mainly delocalized on the TPA core and three inner amido groups, with the highest Mulliken atomic spin density (M–ASD) of ~0.3 single electron on the central N atom (Fig. S33 and Table S4 in Supporting information for the spin density map and the M–ASD values of all atoms in $L_1^{\bullet+}$). The delocalization effects resulted in partial double bond character for the central three C–N single bonds, which accounted for the shortened C–N bond length observed in the radical $Eu_4(L_1^{\bullet+})_4$ cage. Most of the organometallic assemblies reported in the literature were prepared by the reaction of a neutral or an anionic ligand with a cationic metal precursor, while those fabricated by a cationic ligand and metal ions were rare [52,73]. In some cases, transferring the neutral ligand into cationic state even leads to the disassembly of the assemblies [74]. The stability of our assembly may be attributed to the low positive charge density of the radical cation on the tridentate chelating claws, which reduced the cation–cation repulsion between the radical ligand and the Ln^{III} ion.

Luminescence measurements indicated that both L_1 and L_2 can sensitize Tb^{III} (Fig. 3b and Fig. S46 in Supporting information). Taking $Tb_4(L_1)_4$ as an example, upon excitation at 315 nm, a cascade of characteristic emission bands at 618, 583, 543, 488 nm assigning to $^5D_4 \rightarrow {}^7F_J$ ($J = 3-6$) transitions is observed. The longest wavelength absorption maximum of $Tb_4(L_1^{\bullet+})_4$ appears at 740 nm, with a tail that extends beyond 800 nm. It is predictable that $L_1^{\bullet+}$ cannot sensitize $Tb_4(L_1^{\bullet+})_4$ under the same test condition due to low energy levels of the radical species. As shown in Fig. 3b, a broadened band emission centered at 506 nm takes the place of the typical line–like Tb^{III} green luminescence, which probably originated from those recovered neutral ligands in Tb's cage.

The radical stability of $L_1^{\bullet+}$, $La_4(L_1^{\bullet+})_4$ and $Tb_4(L_1^{\bullet+})_4$ was evaluated by monitoring the time–dependent UV–vis absorption spectra under ambient circumstance (Figs. 4a-c). The half–life times ($t_{1/2}$) of $L_1^{\bullet+}$, $La_4(L_1^{\bullet+})_4$ and $Tb_4(L_1^{\bullet+})_4$ were determined to be 53 min, 482 min and 822 min, respectively. The assembly with Ln^{III} ions significantly improved the stability of $L_1^{\bullet+}$, with approximately 9–fold and 15–fold enhancements for La^{III} and Tb^{III} assemblies, respectively (Fig. 4d). The stability of the radical ligands $L_1^{\bullet+}$ could be attributed to the covalent effect, as the incorporation of the ONO chelating moiety to the TPA core enabled the spin density to delocalize to the oxygen atom of inner amide (Fig. S33). Moreover, the coordination of the radical ligands with Ln^{III} ions anchored the radical ligands on the four faces of the tetrahedron, resulting in reduced close stacking of the TPA core and thus enhancing the radical $L_1^{\bullet+}$ stability in the cage. Furthermore, OTf^- and solvent molecules occupied the cavity of the cage and the space between the cages, which prevented the interactions with other reactive molecules, especially O_2, and slowed down decay reactions.

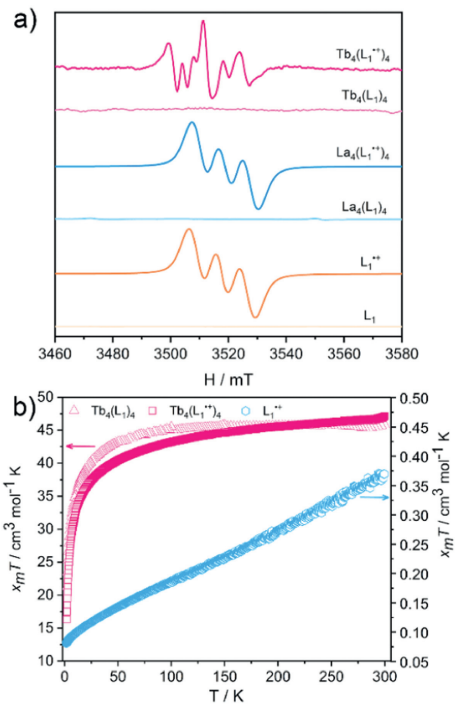

Fig. 5. (a) EPR spectra of ligand L_1 (light yellow line), $L_1^{\bullet+}$ (yellow line, $g = 2.003$), $La_4(L_1)_4$ (light blue line), $La_4(L_1^{\bullet+})_4$ (blue line, $g = 2.003$), $Tb_4(L_1)_4$ (light pink line) and $Tb_4(L_1^{\bullet+})_4$ (pink line, $g = 2.007$) in acetonitrile solution at 293 K. (b) Temperature dependence of $\chi_m T$ for $L_1^{\bullet+}$ (hexagon), $Tb_4(L_1)_4$ (triangle) and $Tb_4(L_1^{\bullet+})_4$ (square) measured at 5000 Oe.

In addition, we found a 1.8-fold increase in $t_{1/2}$ from $La_4(L_1^{\bullet+})_4$ to $Tb_4(L_1^{\bullet+})_4$. To understand this difference, we first consider the influence of lanthanide paramagnetism, thereby EPR spectra under ambient conditions were tested in acetonitrile solution. As shown in Fig. 5a, the EPR spectrum of free ligand $L_1^{\bullet+}$ showed a signal at $g = 2.003$ with a hyperfine structure originating from the nitrogen nuclei ($I = 1$, triplet), indicating that the higher spin density is mainly localized on the central nitrogen atom. Upon complexation with Ln^{III} ($Ln^{III} = La^{III}$ and Tb^{III}) ions, distinct EPR signals were observed, which confirmed the formation of radical $L_1^{\bullet+}$, since the diamagnetic behavior of La^{III} ions and the fast spin–lattice relaxation feature of Tb^{III} ions make both them EPR silent at room temperature [75]. This was further verified by the absence EPR signals for their non–radical counterparts $La_4(L_1)_4$ and $Tb_4(L_1)_4$. These results demonstrated that the radical ligands and assemblies were successfully prepared. Moreover, $La_4(L_1^{\bullet+})_4$ exhibited the same EPR hyperfine signals as the radical ligand $L_1^{\bullet+}$, implying that there was no magnetic interaction between the radical and La^{III} ions or among the four radical ligands themselves. This is reasonable because of the intrinsic diamagnetism of La^{III} ions and the large separation of the central N atoms with higher spin density in the $La_4(L_1^{\bullet+})_4$ tetrahedron (the N–N distance in the Eu^{III} analogue was 6.669 Å). In sharp contrast, six EPR peaks centered at $g = 2.007$ were observed for $Tb_4(L_1^{\bullet+})_4$, which differed from the radical ligand $L_1^{\bullet+}$, suggesting that there was magnetic interaction between Tb^{III} and the organic radical.

To gain a deeper insight into the radical characteristic of $L_1^{\bullet+}$ and the magnetic interaction between Tb^{III} and the radical spins in $Tb_4(L_1^{\bullet+})_4$, direct current (DC) magnetic susceptibilities for the freshly prepared samples of $L_1^{\bullet+}$, $Tb_4(L_1)_4$ and $Tb_4(L_1^{\bullet+})_4$ were recorded in the temperature range of $2-300$ K. As shown in Fig. 5b, the $\chi_m T$ value of $L_1^{\bullet+}$ at 300 K is 0.37 cm^3 K/mol, very close to the expected value for a magnetically isolated system of one $S = 1/2$ with $g = 2.0$ (0.375 cm^3 K/mol), confirming the open shell character of $L_1^{\bullet+}$. The χ_mT values decrease continuously with lowing temperature, indicative of the presence of antiferromagnetic (AF) interaction between adjacent $L_1^{\bullet+}$. For $Tb_4(L_1^{\bullet+})_4$, the experimental χ_mT value at room temperature is 47.13 cm^3 K/mol, quite close to the theoretical value of 48.75 cm^3 K/mol for four non–interacting Tb^{III} ions ($J = 6$, $g = 3/2$) and four magnetically isolated radical spin units. Upon cooling, the $\chi_m T$ values undergo a smooth decrease until about 50 K, below which it decreases rapidly and reaches a minimum value of 16.30 cm^3 K/mol at 2 K. The decrease in low temperature for $Tb_4(L_1^{\bullet+})_4$ is most likely caused by the thermal depopulation of Stark sublevels, but the contribution of AF exchange interactions cannot be ignored. In contrast, the $\chi_m T$ product of $Tb_4(L_1)_4$ maintains roughly constant with lowing temperature down to about 100 K, and then drops to a value of 21.26 cm^3 K/mol at 2 K. This different decrease behavior in $\chi_m T$ *vs.* T curves unambiguously demonstrates the presence of AF coupling between Tb^{III} ion and the radical spin carrier. To further prove the AF interactions, the $\chi_m T$ of $Tb_4(L_1)_4$ is subtracted from the $\chi_m T$ of $Tb_4(L_1^{\bullet+})_4$ to offset the contribution stemming from thermal depopulation of the Stark sublevels of Tb^{III} ions, and the temperature dependence of $\Delta\chi_m T$ ($\Delta\chi_m T = \chi_m T_{(Tb_4(L_1^{\bullet+})_4)} - \chi_m T_{(Tb_4(L_1)_4)}$) is obtained (Fig. S51 in Supporting information). The $\Delta\chi_m$T falls progressively with lowering temperature, confirming again the AF correlations between Tb^{III} ion and radicals. The inherent unquenched orbital angular momentum of Tb^{III} ion together with the delocalization behavior of radical electron make the quantitative estimation of the AF interaction magnitude tricky, which may deserve separate investigation in the future.

Apart from the influence of lanthanide paramagnetism, the Ln radius may also exert effect on the stability of radical $L_1^{\bullet+}$, as the Ln size can affect the rigidity of the ligands and the planarity of the central N atoms. To study this, the $t_{1/2}$ values of $Eu_4(L_1^{\bullet+})_4$, $Gd_4(L_1^{\bullet+})_4$ and $Lu_4(L_1^{\bullet+})_4$ were estimated, giving the $t_{1/2}$ values of 624 min, 1248 min and 347 min, respectively. By comparing the $t_{1/2}$ values with Ln radii (Tables S5 in Supporting information), it was found that the stability of the radical is not dependent on the Ln radius. However, we observed that the assemblies containing diamagnetic Ln ions ($Ln = La^{III}$ and Lu^{III}) show lower $t_{1/2}$ values than those assemblies constructed by paramagnetic Ln assemblies ($Ln = Eu^{III}$, Gd^{III}, Tb^{III}). Based on this observation, we propose that the existence of magnetic interaction between the radical ligands and paramagnetic Ln ions in $Ln_4(L_1^{\bullet+})_4$ ($Ln = Eu^{III}$, Gd^{III} and Dy^{III}) increases the degree of radical electronic delocalization compared to that in $Ln_4(L_1^{\bullet+})_4$ ($Ln = La^{III}$ and Lu^{III}) fabricated by diamagnetic Ln ions, and hence resulting in enhanced radical stability in $Ln_4(L_1^{\bullet+})_4$ ($Ln = Eu^{III}$, Gd^{III} and Dy^{III}).

In summary, we report the first example of a radical–bridged lanthanide organic tetrahedron constructed *via* coordination–driven self–assembly. The progressive stability enhancement of the radical panels was observed from the tetrahedron fabricated by diamagnetic Ln^{III} ions to that by paramagnetic Ln^{III} ions, as certificated by the UV–vis, EPR and magnetic susceptibility measurements. We infer that the enhancement in paramagnetic Ln^{III} ions should be ascribed to the Ln^{III}–radical magnetic interaction, which enables the radical electron more delocalization compared to the Ln^{III} tetrahedron containing diamagnetic Ln^{III} ions. Our findings not only offer some guidance for the preparation of stable radical systems, but also provide new candidates for smart lanthanide materials.

Declaration of competing interest

The authors declare that they have no known competing financial interests or personal relationships that could have appeared to influence the work reported in this paper

Acknowledgments

This work was supported by National Key Research and Development Program of China (Nos. 2021YFA1500400 and 2022YFA1503300), the National Natural Science Foundation of China (Nos. 21825107, 21971237, 22171264 and 22301301) and the Science Foundation of the Fujian Province (No. 2021J02016).

Supplementary materials

Supplementary material associated with this article can be found, in the online version, at doi:10.1016/j.cclet.2024.109641.

References

[1] Y. Sun, C. Chen, J. Liu, et al., Chem. Soc. Rev. 49 (2020) 3889–3919.
[2] E.G. Percastegui, T.K. Ronson, J.R. Nitschke, Chem. Rev. 120 (2020) 13480–13544.
[3] C.M. Hong, R.G. Bergman, K.N. Raymond, et al., Acc. Chem. Res. 51 (2018) 2447–2455.
[4] M.D. Ward, C.A. Hunter, N.H. Williams, Acc. Chem. Res. 51 (2018) 2073–2082.
[5] D.L. Caulder, K.N. Raymond, Acc. Chem. Res. 32 (1999) 975–982.
[6] M. Fujita, M. Tominaga, A. Hori, et al., Acc. Chem. Res. 38 (2005) 369–378.
[7] S. Bai, Y.F. Han, Acc. Chem. Res. 56 (2023) 1213–1227.
[8] C.T. McTernan, J.A. Davies, J.R. Nitschke, Chem. Rev. 122 (2022) 10393–10437.
[9] C.B. Tian, Q.F. Sun, Chem. Eur. J. 29 (2023) e202300195.
[10] Y. Domoto, M. Fujita, Coord. Chem. Rev. 466 (2022) 214605–214617.
[11] F. Wang, S. Bai, Q.W. Zhu, et al., CCS Chem. 5 (2023) 633–640.
[12] K. Acharyya, S. Bhattacharyya, H. Sepehrpour, et al., J. Am. Chem. Soc. 141 (2019) 14565–14569.
[13] P. Howlader, E. Zangrando, P.S. Mukherjee, J. Am. Chem. Soc. 142 (2020) 9070–9078.
[14] M. Pan, K. Wu, J.H. Zhang, et al., Coord. Chem. Rev. 378 (2019) 333–349.
[15] K. Wu, K. Li, S. Chen, et al., Angew. Chem. Int. Ed. 59 (2019) 2639–2643.
[16] J. Zhu, X. Chen, X. Jin, et al., Chin. Chem. Lett. 34 (2023) 108002–108005.
[17] Y.L. Lai, H.J. Zhang, J. Su, et al., Chin. Chem. Lett. 34 (2023) 107686–107690.
[18] C. Li, Y. Wang, Y. Lu, et al., Chin. Chem. Lett. 31 (2020) 1183–1187.
[19] D. Luo, B. Pan, J. Zhang, et al., Chin. Chem. Lett. 32 (2021) 1397–1399.
[20] R.Y. Chen, Y.P. He, J. Zhang, Polyoxometalates 1 (2022) 9140002–9140007.
[21] R.Y. Chen, G.H. Chen, Y.P. He, et al., Chin. J. Struct. Chem. 41 (2022) 2201001–2201006.
[22] X. Liu, X. Feng, K.R. Meihaus, et al., Angew. Chem. Int. Ed. 59 (2020) 10610–10618.
[23] D.J. Bell, L.S. Natrajan, I.A. Riddell, Coord. Chem. Rev. 472 (2022) 214786–214810.
[24] X.Z. Li, C.B. Tian, Q.F. Sun, Chem. Rev. 122 (2022) 6374–6458.
[25] M.H. Du, D.H. Wang, L.W. Wu, et al., Angew. Chem. Int. Ed. 61 (2022) e202200537.
[26] X.L. Li, J. Wu, L. Zhao, et al., Chem. Commun. 53 (2017) 3026–3029.
[27] X.L. Li, J. Wu, J. Tang, et al., Chem. Commun. 52 (2016) 9570–9573.
[28] J. Wang, C. He, P. Wu, et al., J. Am. Chem. Soc. 133 (2011) 12402–12405.
[29] D.E. Barry, D.F. Caffrey, T. Gunnlaugsson, Chem. Soc. Rev. 45 (2016) 3244–3274.
[30] J. Hamacek, A. Vuillamy, Eur. J. Inorg. Chem. 2018 (2017) 1155–1166.
[31] H.Y. Wong, W.S. Lo, K.H. Yim, et al., Chem 5 (2019) 3058–3095.
[32] S.J. Hu, X.Q. Guo, L.P. Zhou, et al., J. Am. Chem. Soc. 144 (2022) 4244–4253.
[33] S.J. Hu, X.Q. Guo, L.P. Zhou, et al., Chin. J. Chem. 41 (2023) 797–804.
[34] B.S. Dolinar, D.I. Alexandropoulos, K.R. Vignesh, et al., J. Am. Chem. Soc. 140 (2018) 908–911.
[35] D.I. Alexandropoulos, B.S. Dolinar, K.R. Vignesh, et al., J. Am. Chem. Soc. 139 (2017) 11040–11043.
[36] X. Liu, Y. Zhang, W. Shi, et al., Inorg. Chem. 57 (2018) 13409–13414.
[37] X. Meng, W. Shi, P. Cheng, Coord. Chem. Rev. 378 (2019) 134–150.
[38] E.T. Seo, R.F. Nelson, J.M. Fritsch, et al., J. Am. Chem. Soc. 88 (1966) 3498–3503.
[39] D.H. Reid, Tetrahedron 3 (1958) 339–352.
[40] S. Kumar, M.R. Ajayakumar, G. Hundal, et al., J. Am. Chem. Soc. 136 (2014) 12004–12010.
[41] P.P. Power, Chem. Rev. 103 (2003) 789–810.
[42] H. Garcia, H.D. Roth, Chem. Rev. 102 (2002) 3947–4007.
[43] V. Pushkara Rao, M.B. Zimmt, N.J. Turro, J. Photochem. Photobio. A: Chem. 60 (1991) 355–360.
[44] H. Hu, Y.Y. Zhang, H. Ma, et al., Angew. Chem. Int. Ed. 62 (2023) e202308513.
[45] E. Breinlinger, A. Niemz, V.M. Rotello, J. Am. Chem. Soc. 117 (1995) 5379–5380.
[46] Q. Song, F. Li, Z. Wang, et al., Chem. Sci. 6 (2015) 3342–3346.
[47] E. Moulin, F. Niess, M. Maaloum, et al., Angew. Chem. Int. Ed. 49 (2010) 6974–6978.
[48] Z. Feng, S. Tang, Y. Su, et al., Chem. Soc. Rev. 51 (2022) 5930–5973.
[49] G. Huo, X. Shi, Q. Tu, et al., J. Am. Chem. Soc. 141 (2019) 16014–16023.
[50] Q. Tu, G.F. Huo, X.L. Zhao, et al., Mat. Chem. Front. 5 (2021) 1863–1871.
[51] S.K. Zhang, L.Z. Ma, W.Q. Ma, et al., Angew. Chem. Int. Ed. 61 (2022) e202209054.
[52] K. Yazaki, S. Noda, Y. Tanaka, et al., Angew. Chem. Int. Ed. 55 (2016) 15031–15034.
[53] Z. Lu, R. Lavendomme, O. Burghaus, et al., Angew. Chem. Int. Ed. 58 (2019) 9073–9077.
[54] G.F. Jin, Y.Z. Zhang, L. Yu, et al., Nano Res. 16 (2023) 10678–10683.
[55] J. Wang, K. Liu, L. Ma, et al., Chem. Rev. 116 (2016) 14675–14725.
[56] G. Tan, X. Wang, Acc. Chem. Res. 50 (2017) 1997–2006.
[57] E. Moulin, J.J.T. Armao, N. Giuseppone, Acc. Chem. Res. 52 (2019) 975–983.
[58] L. Mao, M. Zhou, X. Shi, et al., Chin. Chem. Lett. 32 (2021) 3331–3341.
[59] B. Huang, L. Mao, X. Shi, et al., Chem. Sci. 12 (2021) 13648–13663.
[60] W.L. Jiang, Z. Peng, B. Huang, et al., J. Am. Chem. Soc. 143 (2021) 433–441.
[61] Z.X. Chen, Y. Li, F. Huang, Chem 7 (2021) 288–332.
[62] Ł. Skórka, J.M. Mouesca, J.B. Gosk, et al., J. Mater. Chem. C 5 (2017) 6563–6569.
[63] M. Uebe, T. Kazama, R. Kurata, et al., Angew. Chem. Int. Ed. 56 (2017) 15712–15717.
[64] Y. Yokoyama, D. Sakamaki, A. Ito, et al., Angew. Chem. Int. Ed. 51 (2012) 9403–9406.
[65] X. Li, Y.L. Wang, C. Chen, et al., Chemistry 29 (2023) e202203242.
[66] X. Li, Y.L. Wang, C. Chen, et al., Nat. Commun. 13 (2022) 5367–5374.
[67] X.Q. Guo, L.P. Zhou, L.X. Cai, et al., Chem. Eur. J. 24 (2018) 6936–6940.
[68] L.L. Yan, C.H. Tan, L.P. Zhou, et al., J. Am. Chem. Soc. 137 (2015) 8550–8555.
[69] T. Lu, F. Chen, J. Comput. Chem. 33 (2012) 580–592.
[70] W.Y. Sun, T. Kusukawa, M. Fujita, J. Am. Chem. Soc. 124 (2002) 11570–11571.
[71] K. Sreenath, C.V. Suneesh, V.K. Kumar, et al., J. Org. Chem. 73 (2008) 3245–3251.
[72] S. Zheng, S. Barlow, C. Risko, et al., J. Am. Chem. Soc. 128 (2006) 1812–1817.
[73] Y. Satoh, L. Catti, M. Akita, et al., J. Am. Chem. Soc. 141 (2019) 12268–12273.
[74] V. Croue, S. Goeb, G. Szaloki, et al., Angew. Chem. Int. Ed. 55 (2016) 1746–1750.
[75] J.E. McPeak, S.S. Eaton, G.R. Eaton, Methods Enzymol. 651 (2021) 63–101.